

Spontaneous Capture of Carbohydrate Guests through Folding and Zipping of Self-Assembled Ribbons

Bowen Shen, Ying He, Yongju Kim,* Yanqiu Wang, and Myongsoo Lee*

Abstract: One of the great challenges in molecular self-assembly is how to confer self-folding and closing characteristics on flat two-dimensional structures in response to external triggers. Herein, we report a planar ribbon assembly that folds into closed tubules in response to fructose. The ribbons, ≈ 28 nm wide and 3.5 nm thick, consist of 8 laterally-associated elementary fibrils in which disc-shaped macrocycle amphiphiles are stacked along their axis. Upon addition of fructose, these flat structures spontaneously fold into closed tubules, with an outer diameter of ≈ 8 nm, through zipping of the two sides of the ribbons. Notably, the folding and then zipping of the flat ribbons is accompanied by spontaneous capture of the fructose molecules inside the tubular cavities.

In biological systems, the dynamic folding of flat structures plays a crucial role in initiating many biological functions.^[1] A typical example includes microtubules that are reversibly formed through longitudinal zipping of laterally-associated protofilament sheets triggered by cellular signals.^[2] This dynamic motion gives rise to many important cellular functions, such as organization of intracellular structure and intracellular transport. In addition to its utility for the formation of highly curved tubules with sophisticated functions, the folding motif of a flat structure in nature is of fundamental importance for biological processes such as capture, transport, and release of molecules.^[3] Learning lessons from nature, a challenging target in molecular self-assembly is how to endow dynamic folding to planar structures without compromising their intrinsic features.^[4] The self-assembly of aromatic building blocks provides a facile means to construct flat nanostructures that fold into highly curved objects, such as capsules and tubules.^[5] For example, lateral attachment of the dendritic oligo(ethylene oxide) segments into an aromatic rod causes the molecules to self-assemble into foldable sheets that reversibly roll-up into scrolled tubules in response to thermal energy.^[6] The entropically-driven dehydration of the oligoether chains triggers this structural change to reduce the dehydrated surface area that is exposed to aqueous environments. Recently, we reported that aromatic macrobicycles grafted by hydrophilic oligoether dendrons aggregate to form flat sheets that are able to

spontaneously curve to form hollow capsules.^[7] The curvature of the self-assembled sheets arises from the intercalation of curved corannulene guests into a macrocycle bilayer. An additional example of flat structures include ribbons that are able to be rolled or twisted to form curved structures, mediated, in many cases, by a twisted packing of chiral subunits.^[8] Many other examples of ribbon structures maintaining a flat conformation have been reported, including those based on short oligopeptides,^[9] lipid molecules,^[10] perylene dyes,^[11] and rod amphiphiles.^[12] Nonetheless, most of the flat structures do not display highly controlled folding and subsequent zipping to form closed structures with hollow inner cavities in response to external triggers.^[13]

Herein, we report self-assembled ribbons in methanol that fold into closed tubules in response to addition of fructose. The flat ribbon structures are composed of laterally assembled elementary fibrils in which disc-shaped macrocycles are stacked along their axis. Upon addition of carbohydrate, these flat structures spontaneously curve into closed tubules through zipping of the two sides of the ribbons. The zipping after folding of the flat ribbons is accompanied by spontaneous capture of fructose molecules inside the tubular cavities (Figure 1). The molecular subunits stacked into the elemen-

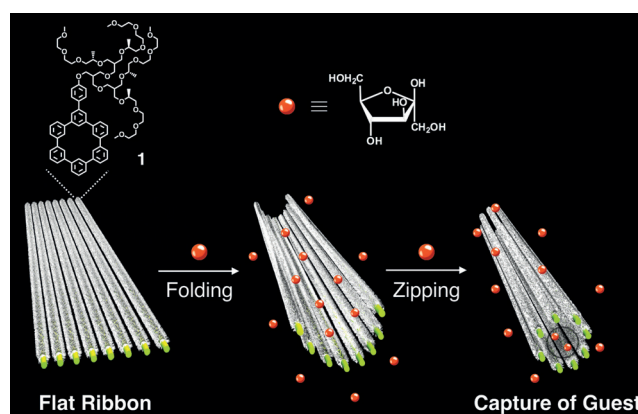


Figure 1. Molecular structure of macrocyclic amphiphile **1** and representation of the ribbon folding and then zipping into a tubule driven by fructose.

tary fibrils consist of a cyclohexa-*m*-phenylene aromatic segment and an oligoether dendron at the aromatic periphery. Shape-persistent aromatic macrocycles have a strong tendency to stack on top of each other to generate columnar fibrils that laterally associate to form various higher order structures.^[14] Therefore, we expected that the cyclohexa-*m*-phenylene unit generates long fibrils surrounded by flexible

[*] B. Shen, Y. He, Dr. Y. Kim, Y. Wang, Prof. M. Lee
State Key Laboratory of Supramolecular Structure and Materials
College of Chemistry, Jilin University
Changchun 130012 (China)
E-mail: mslee@jlu.edu.cn
yjkim@jlu.edu.cn

Supporting information for this article is available on the WWW under <http://dx.doi.org/10.1002/anie.201509190>.

chains, which are able to further associate in a side-by-side fashion. To control the lateral association of the elementary columnar stacks and endow the molecules with amphiphilic features, we incorporated a hydrophilic oligoether dendron into the aromatic periphery. Amphiphilic molecule **1**, based on a discotic macrocycle, was synthesized from commercially available starting materials according to the procedures reported previously (Supporting Information, Figures S1 and S2).^[15] The self-assembling behavior of the molecule was investigated in methanol using transmission electron microscopy (TEM) and atomic force microscopy (AFM). The microscopic investigations showed that the macrocycle amphiphile self-assembles into well-defined planar structures with a uniform lateral dimension.

Detailed investigations of the methanol solutions of **1** (0.01 wt %) by TEM revealed flat ribbon structures with a uniform width of ≈ 28 nm and a length of several hundred nanometers (Figure 2a). The magnified image showed that

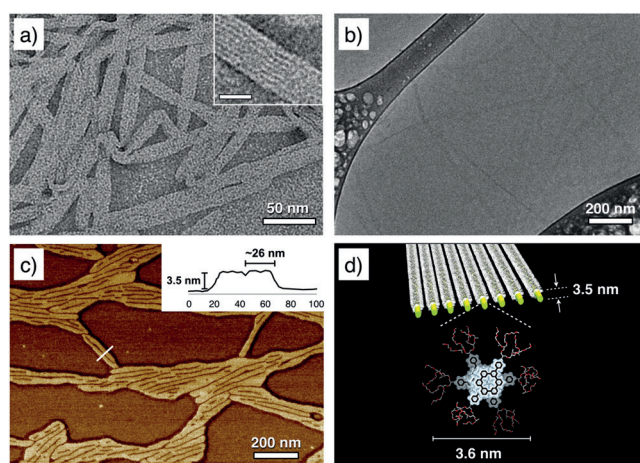


Figure 2. Self-assembled ribbon structures of **1** from 0.01 wt % methanol solution. a) TEM image stained with uranyl acetate. The inset shows magnified image. Inset scale bar = 20 nm. b) Cryo-TEM image of **1** from 0.01 wt % in methanol solution. c) AFM image of **1** from 0.01 wt % in methanol solution. (inset: the height profile along white line, height: 3.5 nm; width: ≈ 26 nm). d) Representation of the dimensions of ribbon and the interdigitated bilayer packing of **1** in elementary fibrils.

the ribbon consists of longitudinal stripes with a regular spacing of 3.6 nm, demonstrating that the ribbon assembly originates from the lateral association of ≈ 8 preformed fibrils (Figure 2a, inset), similar to laterally associated protofilament sheets of microtubules.^[2] The formation of the flat nanostructures was also confirmed using cryo-TEM with the vitrified methanol solution, which provides further evidence that the aggregates exist as planar ribbons in bulk solution (Figure 2b and Figure S3). To gain insight into the formation of the flat ribbon structure, we performed TEM experiments with a highly diluted solution (0.002 wt %) of **1** (Figure S4). The images showed thin fibrils with a uniform diameter of 3.8 nm, further indicating that the ribbons consist of the lateral association of the elementary fibrils. Additional structural information on the ribbons was obtained by

atomic force microscopy (AFM) measurement on a hydrophilic mica substrate in the completely dried state (Figure 2c and Figure S5). The AFM image of **1** revealed planar ribbons with a thickness of 3.5 nm, which is consistent with the expected thickness of interdigitated bimolecular packing (Figure 2d). These observations indicate that, at the initial stages of the self-assembly process, the aromatic macrocycles stack on top of one another to form a long fibril, 3.6 nm in diameter, surrounded by oligoether chains. However, the aromatic scaffolds of the fibrils are not entirely surrounded by oligoether chains, according to the molecular modeling. As a result, the elementary fibrils further assemble through side by side interactions to generate a planar ribbon structure with a width of ≈ 28 nm, which is composed of ≈ 8 laterally bound fibrils (Figure 1). The uniform ribbon formation is believed to arise from a delicate balance between the energetic gain by lateral association and the resulting entropic penalty for splaying the flexible dendritic segments.^[16]

The lateral associations of the aromatic fibrils based on symmetric molecules or symmetric bimolecular packings give rise to the formation of flat 2-D structures with symmetric up and down basal planes, resulting in high stability against bending.^[11,17] However, although symmetric bimolecular packing is more stable, the aromatic macrocycle of **1** is able to readily rotate with respect to the neighbouring macrocycles in columnar stacks, owing to the relatively low rotational energy barrier, to generate asymmetric locations of flexible chains around the aromatic scaffolds, giving rise to asymmetric bimolecular packings (Figure 3a). To investigate the influence of the solvent polarity between symmetric and asymmetric bimolecular packing modes, we performed COSMO/DFT energy calculations based on a series of dielectric constants, such as 32.6 (methanol), 40, 50, 60, 70, and 78.5 (water). Interestingly, asymmetric packing shows larger stabilization energies with increasing dielectric constant values than those of symmetric packing (Figure 3b and Figure S6). These patterns are attributed to the larger dipole moment of asymmetric packing, which is favored in polar solvent (Figure 3a). Therefore, a ratio of asymmetric packing arises from the increase of the dielectric constant, and it induces the curvature in the lateral association of the columnar fibrils.

When the planar ribbons are faced with poor solvent environments, the dynamic placements of the oligoether chains around the aromatic columnar scaffolds are expected to enforce the planar ribbon structure to be folded lengthwise to minimize surface tension.^[18] This led us to envision that the planar ribbons arising from the parallel association of the columnar fibrils would be spontaneously folded into closed tubules through lengthwise zipping in response to the addition of a carbohydrate which endows increased solvophobic environments with the oligoether-coated ribbon structures.^[19] We thus investigated the structural transformation of the planar ribbons upon carbohydrate addition into the methanol solution.

To corroborate carbohydrate-mediated deformation of the planar ribbons, we selected the methanol-soluble carbohydrate fructose, which is also an attractive renewable source for the production of biofuels and bio-based chemicals.^[20]

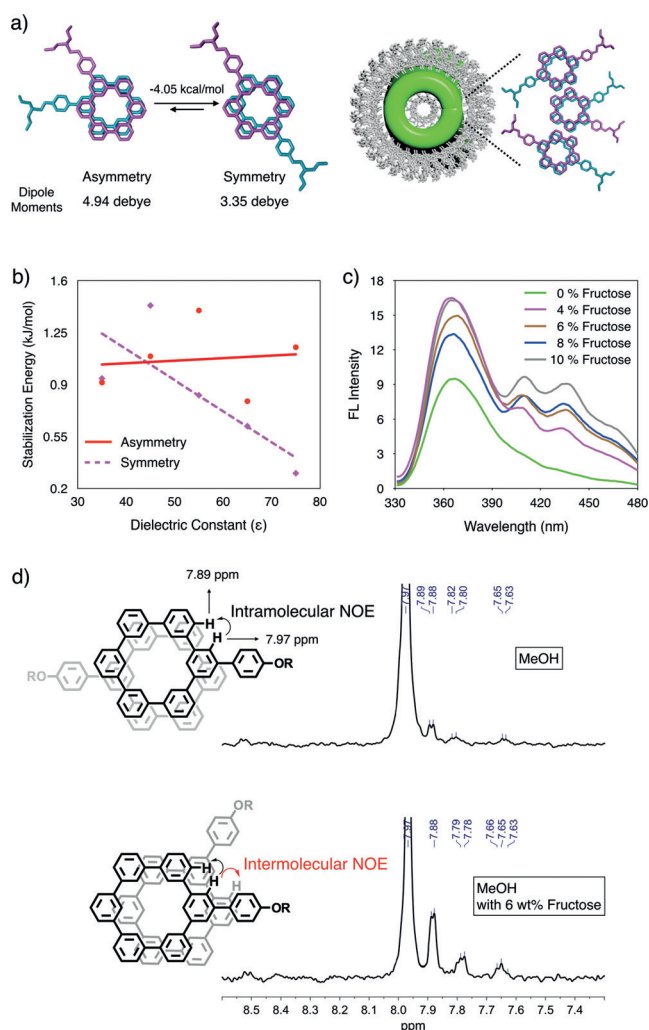


Figure 3. a) DFT energy calculations between asymmetric and symmetric bimolecular packings shows that asymmetric packing have a higher energy and a dipole moment value. b) COSMO/DFT energy calculation shows that asymmetric bimolecular packing gives the larger stabilization energies upon increase of dielectric constant than those of symmetric packing. c) The emission spectra of **1** in methanol solution (0.01 wt%) with different concentrations of fructose. Wavelength for excitation = 250 nm. d) 1D NOE spectra of **1** from 0.05 wt% CD_3OD solution with and without 6 wt% fructose. Irradiation at 7.97 ppm.

Upon addition of fructose into a methanol solution of **1** (0.01 wt%), the absorption maximum is slightly red-shifted and the intensity decreases with respect to those observed in pure methanol (Figure S7). Notably, the fluorescence spectra upon fructose addition revealed fluorescence enhancement at 365 nm together with prominent emissions at longer wavelengths centered at 440 nm. (Figure 3b). These additional emission peaks likely arise from an excimer-like emission associated with the strong intermolecular electronic interactions of the closely-packed aromatic segments.^[21] These results indicate that fructose enforces the disc-shaped aromatic segments to be packed more closely, owing to the enhanced solvophobic effect driven by more favored interactions between fructose and methanol, compared to the oligoether chains.^[22]

To gain further insight into the aromatic interactions, one-dimensional (1D) nuclear Overhauser effect (NOE) measurements were performed in CD_3OD solutions with and without 6 wt% fructose (Figure 3c and Figure S8). When the proton at 7.97 ppm was irradiated in CD_3OD solutions, NOE peaks were detected at 7.89, 7.80, and 7.64 ppm, respectively, indicating the proximity of ^1H nuclei in space. Upon the addition of fructose (6 wt%) to the methanol solution, however, the intensities of the NOE peaks were increased, demonstrating that fructose forces the aromatic segments to be stacked more closely. This result is consistent with the induction of the excimer-like emission upon fructose addition. Notably, the enhancement of the NOE intensity at 7.89 ppm is more prominent compared to the other NOE peaks, which is attributed to asymmetric bimolecular packings.^[23] These results demonstrate that the solvophobic effect arising from the fructose addition drives the flat ribbons to be curved through the formation of asymmetric bilayers, as described earlier (Figure 3a).

The closer packings of the aromatic segments upon fructose addition would lead to the structural deformation of the flat ribbons through molecular rearrangements. To corroborate a fructose-mediated structural change, we performed TEM experiments with the 0.01 wt% methanol solution of **1** containing 6 wt% fructose. Notably, TEM images showed hollow tubular objects with an outer diameter of ≈ 8 nm, indicating that fructose forces the planar ribbons to be folded into hollow tubules (Figure 4a). Closer examinations exhibit a dark interior separated by white periphery, demonstrating that the individual fibers are based on hollow tubules (Figure 4a, inset). Considering the measured tubular diameter of 8 nm and the ribbon thickness of 3.5 nm, the internal pore size of the tubule is estimated to be ≈ 1 nm. An interesting point to note is that the observed tubular diameter provides the circumference of the cross-sectional tubular

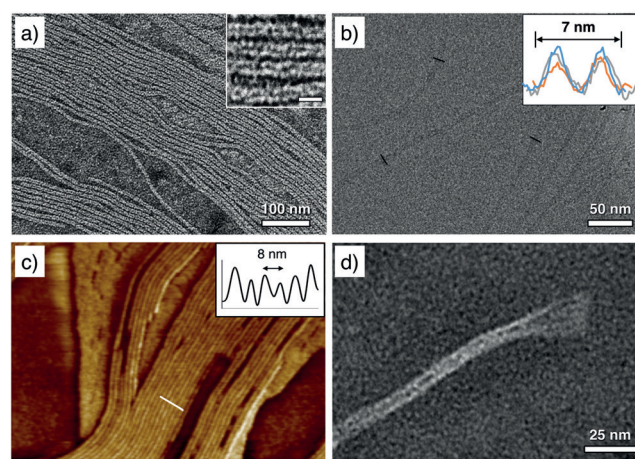


Figure 4. a) Negatively-stained TEM image of **1** from 0.01 wt% methanol solution including 6 wt% fructose. The inset is a magnified image. Inset scale bar = 10 nm. b) Cryo-TEM (inset is electron density profiles denoted by the blank line) and c) AFM image (inset is the cross-section profile denoted by the white line) of **1** from 0.01 wt% methanol solution including 6 wt% fructose. d) Negatively-stained TEM image from 0.01 wt% **1** in the methanol solution containing 2 wt% fructose without aging.

circle to be 25 nm, which indicates a $\approx 10\%$ reduction with respect to the ribbon width (≈ 28 nm). This size reduction in lateral dimension further supports that fructose forces the parallel arrangement of the elementary fibrils as well as the aromatic stackings to be more closely packed through the strengthened solvophobic interactions. The formation of the hollow tubules in bulk solution was also confirmed using cryo-TEM with the vitrified solutions, which revealed fiber-like structures with a diameter of 7 nm (Figure 4b). This mismatch in diameter originates from solvated ethylene oxide chains, which do not provide enough contrast for direct observations.^[24] The hollow interior was evidenced by the different contrasts between the periphery and center of the fiber-like structures, which is characteristic of a tubular structure.^[25]

The structural transformation was also confirmed by AFM measurements on hydrophilic mica substrates in the completely dried state (Figure 4c). The image derived from fructose addition revealed closely packed, fiber-like aggregates with a diameter of 8 nm, in contrast to that based on pure methanol solution. This structural transformation is consistent with the results obtained from TEM. To understand the transformation mechanism of the tubules, we additionally performed TEM experiments with the methanol solution containing 2 wt % fructose without aging (Figure 4d and Figure S9). The images showed that the ribbons are curved along the long axis which, in turn, zipped into the closed tubular structures. These results demonstrate that fructose drives the planar ribbons to be folded lengthwise and then zipped into closed tubular structures (Figure 1).

The folding of the flat ribbons can be understood by considering the solvophobic effect endowed with fructose, as described earlier. Upon addition of highly hydrophilic fructose, the methanol solution would change into a poor solvent environment for the oligoether-coated planar ribbon structures because the hydrogen bonding interactions between carbohydrate and methanol are stronger than its interactions with the oligoethylene oxide chains.^[22,26] The poor solvent environment leads the aromatic segments of the oligoether-coated nanostructures to be more closely packed, as reflected in the appearance of excimer-like emission, the size reduction in lateral dimension of the ribbons, and the increased NOE signals of the aromatic segments in ^1H NMR. To minimize the surface energy generated by the poor solvent environment, the flat ribbons would be curved in a perpendicular direction to the ribbon axis through asymmetric redistribution of the oligoether chains located at the up and down basal planes. Subsequently, the two sides of the folded ribbon are zipped along the long axis to form closed tubules to reduce the exposure of the aromatic segments in edge parts toward a poor solvent environment, which is evidenced in the intermediate structures observed by TEM (Figure 4d).

Importantly, the folding and lengthwise zipping of the ribbons spontaneously captures the fructose in the solution. The capture of the fructose through the folding of ribbons was confirmed by tracing HPLC after separation of the free fructose from the tubular solution (6 wt % fructose) using a Sephadex column. An additional peak corresponding to the encapsulated fructose (0.9%) was clearly identified in the fraction profile from the Sephadex column chromatogram

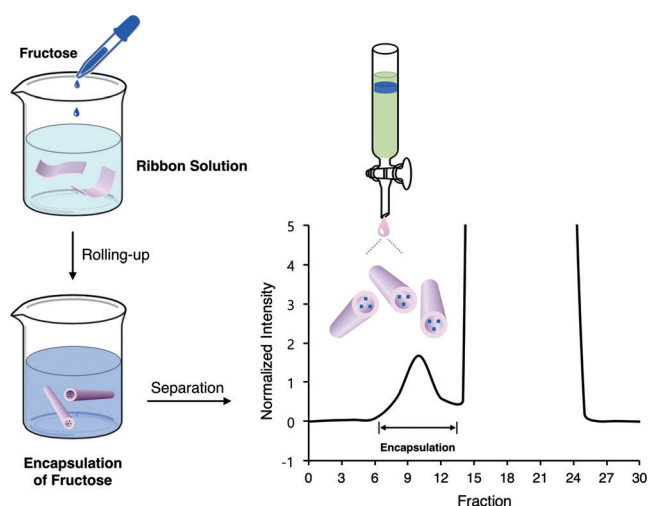


Figure 5. After rolling-up of the ribbons by the addition of fructose, the encapsulated fructose was subjected to separation with Sephadex column. The fraction of eluate was monitored to measure the amount of fructose in each fraction.

(Figure 5), demonstrating that the fructose in the methanol solution is spontaneously captured inside the tubular cavities through the folding and zipping actions of the planar ribbons.

The results described herein demonstrate that the self-assembly of the disc-shaped aromatic amphiphile generates long columnar fibrils that laterally associate to form planar ribbons. The ribbons have 8 laterally associated elementary fibrils, and are ≈ 28 nm wide and 3.5 nm thick. Notably, these flat structures spontaneously curve into closed tubules with an outer diameter of ≈ 8 nm through lengthwise folding and then zipping driven by fructose addition. The zipping after folding is accompanied by spontaneous capture of fructose dissolved in the solution. Considering that most of the planar structures are far from the guest wrapping through folding and zipping,^[27] the most notable feature of our ribbon structures is their ability to spontaneously capture guest molecules through folding and then zipping actions in response to guest addition. The driving force responsible for the folding and zipping of the planar structures is believed to be the solvophobic effect generated by increased carbohydrate–methanol interactions that would decrease methanol–nanoscale structure interactions, a similar effect to preferential exclusion.^[26] Such a unique folding of the flat structures to create nanoscale containers may provide new opportunities for using 2D structures to capture specific biomolecules in a size-selective manner by wrapping and transferring them to their target for a variety of applications.

Acknowledgements

This work was supported by 1000 program, NSFC (grants 51473062 and 21450110416).

Keywords: carbohydrate capture · lengthwise folding · ribbon structure · self-assembly · zipping

How to cite: *Angew. Chem. Int. Ed.* **2016**, *55*, 2382–2386
Angew. Chem. **2016**, *128*, 2428–2432

- [1] a) B. J. Reynwar, G. Illya, V. A. Harmandaris, M. M. Müller, K. Kremer, M. Deserno, *Nature* **2007**, *447*, 461–464; b) J. Zimmerberg, M. M. Kozlov, *Nat. Rev. Mol. Cell Biol.* **2006**, *7*, 9–19.
- [2] a) C. Conde, A. Caceres, *Nat. Rev. Neurosci.* **2009**, *10*, 319–332; b) A. Szyk, A. M. Deaconescu, J. Spector, B. Goodman, M. L. Valenstein, N. E. Ziolkowska, V. Kormendi, N. Grigorieff, A. Roll-Mecak, *Cell* **2014**, *157*, 1405–1415.
- [3] H. T. McMahon, J. L. Gallop, *Nature* **2005**, *438*, 590–596.
- [4] a) S. Pandey, M. Ewing, A. Kunas, N. Nguyen, D. H. Gracias, G. Menon, *Proc. Natl. Acad. Sci. USA* **2011**, *108*, 19885–19890; b) K.-U. Jeong, J.-H. Jang, D.-Y. Kim, C. Nah, J. H. Lee, M.-H. Lee, H.-J. Sun, C.-L. Wang, S. Z. D. Cheng, E. L. Thomas, *J. Mater. Chem.* **2011**, *21*, 6824–6830; c) L. M. Viculis, J. J. Mack, R. B. Kaner, *Science* **2003**, *299*, 1361; d) W. Cai, C. Y. Li, L. Li, B. Lotz, M. Keating, D. Marks, *Adv. Mater.* **2004**, *16*, 600–605; e) H. M. White, I. L. Hosier, D. C. Bassett, *Macromolecules* **2002**, *35*, 6763–6765.
- [5] a) D.-J. Hong, E. Lee, H. Jeong, J.-K. Lee, W.-C. Zin, T. D. Nguyen, S. C. Glotzer, M. Lee, *Angew. Chem. Int. Ed.* **2009**, *48*, 1664–1668; *Angew. Chem.* **2009**, *121*, 1692–1696; b) J.-K. Kim, E. Lee, Y.-b. Lim, M. Lee, *Angew. Chem. Int. Ed.* **2008**, *47*, 4662–4666; *Angew. Chem.* **2008**, *120*, 4740–4744; c) X. Zhang, S. Rehm, M. M. Safont-Sempere, F. Würthner, *Nat. Chem.* **2009**, *1*, 623–629; d) A. Ajayaghosh, R. Varghese, V. K. Praveen, S. Mahesh, *Angew. Chem. Int. Ed.* **2006**, *45*, 3261–3264; *Angew. Chem.* **2006**, *118*, 3339–3342; e) S. Yagai, Y. Nakano, S. Seki, A. Asano, T. Okubo, T. Isoshima, T. Karatsu, A. Kitamura, Y. Kikkawa, *Angew. Chem. Int. Ed.* **2010**, *49*, 9990–9994; *Angew. Chem.* **2010**, *122*, 10186–10190.
- [6] E. Lee, J.-K. Kim, M. Lee, *Angew. Chem. Int. Ed.* **2009**, *48*, 3657–3660; *Angew. Chem.* **2009**, *121*, 3711–3714.
- [7] Y. Kim, M. Lee, *Chem. Eur. J.* **2015**, *21*, 5736–5740.
- [8] a) L. Ziserman, H.-Y. Lee, S. R. Raghavan, A. Mor, D. Danino, *J. Am. Chem. Soc.* **2011**, *133*, 2511–2517; b) A. Brizard, C. Aimé, T. Labrot, I. Huc, D. Berthier, F. Artzner, B. Desbat, R. Oda, *J. Am. Chem. Soc.* **2007**, *129*, 3754–3762; c) T. Shimizu, M. Masuda, H. Minamikawa, *Chem. Rev.* **2005**, *105*, 1401–1443; d) W.-Y. Yang, E. Lee, M. Lee, *J. Am. Chem. Soc.* **2006**, *128*, 3484–3485; e) C. B. Winiger, S. M. Langenegger, G. Calzaferri, R. Häner, *Angew. Chem. Int. Ed.* **2015**, *54*, 3643–3647; *Angew. Chem.* **2015**, *127*, 3714–3718.
- [9] M. S. Lamm, K. Rajagopal, J. P. Schneider, D. J. Pochan, *J. Am. Chem. Soc.* **2005**, *127*, 16692–16700.
- [10] L. Moreau, P. Barthélémy, M. E. Maataoui, M. W. Grinstaff, *J. Am. Chem. Soc.* **2004**, *126*, 7533–7539.
- [11] X. Zhang, D. Görl, V. Stepanenko, F. Würthner, *Angew. Chem. Int. Ed.* **2014**, *53*, 1270–1274; *Angew. Chem.* **2014**, *126*, 1294–1298.
- [12] a) S. Yagai, T. Kinoshita, Y. Kikkawa, T. Karatsu, A. Kitamura, Y. Honsho, S. Seki, *Chem. Eur. J.* **2009**, *15*, 9320–9324; b) E. R. Zubarev, M. U. Pralle, E. D. Sone, S. I. Stupp, *J. Am. Chem. Soc.* **2001**, *123*, 4105–4106; c) E. Lee, Z. Huang, J.-H. Ryu, M. Lee, *Chem. Eur. J.* **2008**, *14*, 6957–6966; d) E. Lee, J.-K. Kim, M. Lee, *Angew. Chem. Int. Ed.* **2008**, *47*, 6375–6378; *Angew. Chem.* **2008**, *120*, 6475–6478.
- [13] a) N. Patra, B. Wang, P. Král, *Nano Lett.* **2009**, *9*, 3766–3771; b) D. V. Kosynkin, A. L. Higginbotham, A. Sinititskii, J. R. Lomeda, A. Dimiev, B. K. Price, J. M. Tour, *Nature* **2009**, *458*, 872–877.
- [14] a) X. Zhou, G. Liu, K. Yamato, Y. Shen, R. Cheng, X. Wei, W. Bai, Y. Gao, H. Li, Y. Liu, F. Liu, D. M. Czajkowsky, J. Wang, M. J. Dabney, Z. Cai, J. Hu, F. V. Bright, L. He, X. C. Zeng, Z. Shao, *Nat. Commun.* **2012**, *3*, 949; b) S. Rondeau-Gagné, J. Roméo Néabo, M. Desroches, I. Levesque, M. Daigle, K. Cantina, J.-F. Morin, *Chem. Commun.* **2013**, *49*, 9546–9548; c) S. Rosselli, A.-D. Ramminger, T. Wagner, G. Lieser, S. Höger, *Chem. Eur. J.* **2003**, *9*, 3481–3491.
- [15] a) Z. Huang, S.-K. Kang, M. Banno, T. Yamaguchi, D. Lee, C. Seok, E. Yashima, M. Lee, *Science* **2012**, *337*, 1521–1526; b) W. Pisula, M. Kastler, C. Yang, V. Enkelmann, K. Müllen, *Chem. Asian J.* **2007**, *2*, 51–56; c) Y. Kim, J. Kang, B. Shen, Y. Wang, Y. He, M. Lee, *Nat. Commun.* **2015**, *6*, 8650.
- [16] a) M. A. Horsch, Z. Zhang, S. C. Glotzer, *Nano Lett.* **2006**, *6*, 2406–2413; b) D. J. Hong, E. Lee, J. K. Lee, W. C. Zin, M. Han, E. Sim, M. Lee, *J. Am. Chem. Soc.* **2008**, *130*, 14448–14449.
- [17] T. M. Birshtein, P. A. Iakovlev, V. M. Amoskov, F. A. M. Leermakers, E. B. Zhulina, O. V. Borisov, *Macromolecules* **2008**, *41*, 478–488.
- [18] J. C. Nelson, J. G. Saven, J. S. Moore, P. G. Wolynes, *Science* **1997**, *277*, 1793–1796.
- [19] J. Malsam, A. Aksan, *J. Phys. Chem. B* **2009**, *113*, 6792–6799.
- [20] R.-J. van Putten, J. C. van der Waal, E. de Jong, C. B. Rasrendra, H. J. Heeres, J. G. de Vries, *Chem. Rev.* **2013**, *113*, 1499–1597.
- [21] G. A. Sherwood, R. Cheng, K. Chacon-Madrid, T. M. Smith, L. A. Peteanu, *J. Phys. Chem. C* **2010**, *114*, 12078–12089.
- [22] R.-J. Van Putten, J. G. M. Winkelman, F. Keihan, J. C. Van der Waal, E. De Jong, H. J. Heeres, *Ind. Eng. Chem. Res.* **2014**, *53*, 8285–8290.
- [23] D. Görl, X. Zhang, V. Stepanenko, F. Würthner, *Nat. Commun.* **2015**, *6*, 7009.
- [24] Y. He, Z. Li, P. Simone, T. P. Lodge, *J. Am. Chem. Soc.* **2006**, *128*, 2745–2750.
- [25] S. Sengupta, D. Ebeling, S. Patwardhan, X. Zhang, H. von Berlepsch, C. Böttcher, V. Stepanenko, S. Uemura, C. Hentschel, H. Fuchs, F. C. Grozema, L. D. A. Siebbeles, A. R. Holzwarth, L. Chi, F. Würthner, *Angew. Chem. Int. Ed.* **2012**, *51*, 6378–6382; *Angew. Chem.* **2012**, *124*, 6484–6488.
- [26] C. Özdemir, A. Güner, *Eur. Polym. J.* **2007**, *43*, 3068–3093.
- [27] R. Fernandes, D. H. Gracias, *Adv. Drug Delivery Rev.* **2012**, *64*, 1579–1589.

Received: October 1, 2015

Revised: November 22, 2015

Published online: January 14, 2016